

# Gravelamps: Gravitational Wave Lensing Mass Profile Model Selection

MICK WRIGHT<sup>1</sup> AND MARTIN HENDRY<sup>1</sup>

<sup>1</sup>*SUPA, School of Physics and Astronomy, University of Glasgow*

## ABSTRACT

We present the package GRAVELAMPS which is designed to analyse lensed gravitational wave signals in order to constrain the mass density profile of the lensing object. GRAVELAMPS does this via parameter estimation using the framework of BILBY, which enables estimation of both the lens and the source parameters. The package can be used to study both microlensing and macrolensing cases – where the lensing mass distribution is described by a point mass and extended mass density profile respectively – and allows the user to easily and freely switch between the full wave optics and approximate geometric optics descriptions, which are applied to each of these cases. The performance of GRAVELAMPS is demonstrated via simulated analysis of both a microlensing and macrolensing event, illustrating its capability for both parameter estimation and model selection. To further demonstrate the utility of the package, the real gravitational-wave event GW170809 was analysed using GRAVELAMPS; this event was found to yield no strong evidence supporting the lensing hypothesis, consistent with previously published results.

## 1. INTRODUCTION

For most of the time that we have spent observing the universe, we have been able to do so using only the electromagnetic (EM) spectrum – firstly via the visible window and then in the 20th century expanding to cover the full range from gamma rays to radio. However, with the dawn of gravitational-wave astronomy and the first detections of signals from the mergers of compact binary systems made by LIGO (Aasi et al. 2015) and VIRGO (Acernese et al. 2014), we have now opened an entirely new gravitational-wave window on the universe. The detection of gravitational waves was the culmination of a century of research, from the first theoretical description of the phenomenon (Einstein 1916) in 1916 up to the observation of GW150914 (Abbott et al. 2016), and onwards – with now more than 50 confirmed detections (Abbott et al. 2019) (The LIGO Scientific Collaboration et al. 2021) (Abbott et al. 2021), and the prospect of many hundreds more as the extended 2nd-generation ground-based detector network reaches its design sensitivity later this decade.

In addition to the development of the ground-based detectors themselves, in recent years a great deal of work has gone into creating computational tools capable of generating predicted gravitational waveforms and comparing them to the interferometer data, in order to detect sources and infer their parameters – as discussed in more detail in Abbott et al. (2020). Two extensive toolkits of particular importance are the LIGO Algorithm Library, or LAL (LIGO Scientific Collaboration

2018), and BILBY (Ashton et al. 2019): the former allows the straightforward generation of many different types of waveform, as just one of its many functionalities, whilst the latter presents an easy interface with which to perform the aforementioned parameter estimation using a variety of nested sampling (Skilling 2004) (Skilling 2006) algorithms.

A recent focus of attention for the nascent field of gravitational-wave astronomy has been the gravitational lensing of gravitational waves (The LIGO Scientific Collaboration & The Virgo Collaboration 2021) (Broadhurst et al. 2019) (Diego, J. M. et al. 2019) (Janquart et al. 2021) (Seo et al. 2021) (Cremonese et al. 2021), (Mukherjee et al. 2021), (Ezquiaga et al. 2021), (Xu et al. 2021) (Chung & Li 2021). Just as light passing by a massive compact object is deflected by the warping of space-time, so too gravitational wave signals are affected by the distribution of intervening matter as they propagate towards us. Electromagnetic observations of gravitational lensing have played an important role in the development of general relativity, with the deflection of light being one of its four major tests (Dyson et al. 1923). In a similar way, it is hoped that future observations of the lensing of gravitational waves may prove to be not just an important further test of general relativity and other theories of gravity, but also a powerful diagnostic probe of the nature of dark matter (Mishra et al. 2021) (Urrutia & Vaskonen 2021).

Dark matter, as the name implies, can only be probed indirectly using light. Nevertheless, for several decades powerful tools have been developed and applied to re-

construct the distribution of dark matter using EM observations of gravitational lensing (Schneider 1996) (Amorisco et al. 2021) and a number of authors have recognised that observations of lensed gravitational-wave signals may provide a valuable adjunct to the information and constraints yielded by EM observations alone (Wang et al. 2021). In particular, several authors have investigated how the mass density profile of the lensing dark matter will affect the observed properties of the lensed gravitational-wave profile (Cao et al. 2014) (Takahashi & Nakamura 2003), and have sought to demonstrate how these properties may be used to characterise lensed events and hence constrain the parameters of the lens model (Herrera-Martín et al. 2019) (Mishra et al. 2021).

Extending the above work, presented here is the package GRAVELAMPS, which is designed to analyse gravitational-wave data fitted to arbitrary lens models. Built upon the LAL and BILBY frameworks, GRAVELAMPS performs parameter estimation on gravitational-wave strain data for a range of different mass density profile models, yielding estimates for the joint posterior distribution of the lens and source parameters of each model and also estimating the Bayesian evidence for that model. Comparing these evidences for different models allow calculation of the Bayes Factor, which quantifies how probable is one model is compared to another, thus providing a means to quantitatively evaluate which mass profile for the lens is the most likely.

In the following sections, the reader will be guided through the theory behind GRAVELAMPS and its usage, performance, and design sensibilities, as well as some example results from the package to illustrate how it might be applied to differing scenarios – including descriptions of some potential future additions as well as ways in which it could be integrated into the already extant detection pipelines for lensing. Section 2 will cover the theory of gravitational lensing in general, Section 3 will cover the specific profiles that are presently integrated into GRAVELAMPS, Section 4 will develop upon this to describe the calculation of the amplification factor, Section 5 will then go into more detail about the code itself – giving more detailed explanations of how it was constructed and how it can be used. Section 6 will then present some results from usage of GRAVELAMPS in a variety of possible scenarios. Finally, Section 7 will conclude and give some of the aforementioned detail on possible future extensions, as well as integration of the code into existing analysis pipelines.

## 2. GRAVITATIONAL WAVE LENSING THEORY

Gravitational lensing is a phenomenon predicted by General Relativity. The curvature of space-time is affected by the presence of massive objects in the universe and this curvature influences the path followed by a beam of light or a gravitational wave as it propagates: as the beam passes by a massive object, it follows a curved path. This bending of light or gravitational waves is qualitatively similar to that produced by optical lenses – hence the name gravitational lensing. Proving that such light deflection was indeed occurring, and by the amount described by the theory, was one of the four major tests of General Relativity. This test was successfully carried out for light in 1919 in the renowned Eddington Experiment, in which the angle of deflection of starlight passing very close to the limb of the Sun was measured to be consistent with the amount predicted by GR (Dyson et al. 1923).

Since that initial detection, thousands of examples of lensing have been observed and the phenomenon has firmly entered the astronomers’ toolkit as a powerful tool for analysing the distant cosmos. One notable recent example is the so-called ‘Cosmic Horseshoe’ (Belokurov et al. 2007), which was detected as part of the Sloan Digital Sky Survey and of which an image was then captured using the Hubble Space Telescope, showing the distortion of one galaxy by another – creating two separate stretched images resembling a horseshoe.

Gravitational lensing has, by now, been routinely observed across the electromagnetic spectrum, but in principle the phenomenon will also affect gravitational-wave observations. Building upon several decades of theoretical studies of gravitational-wave lensing, following the first direct detection of gravitational-waves in 2015, a major effort has begun to search for evidence of gravitational lensing observed in the gravitational-wave signals that have thus far been detected by the network of ground-based interferometers (Hannuksela et al. 2019) (The LIGO Scientific Collaboration & The Virgo Collaboration 2021). We now briefly review the relevant theoretical foundations that underpin these developments.

### 2.1. Lens Equation

To outline the theory of gravitational lensing, and to consider how it affects a gravitational-wave signal, we begin with a simple system where the propagation of the wave can be adequately described by geometrical optics. Consider a source,  $S$ , which is displaced from the optical axis by a distance  $\eta$  and is lensed by an object of mass,  $M$  at an angle  $\hat{\alpha}$ . Rays emitted from this source will be deflected by the mass  $M$ , creating an image,  $I$ , the apparent position of which will be displaced with respect to  $S$ . Given this deflection, the observer can define two

angles:  $\theta$  which is the angle between the observer and the image, and  $\beta$  which is the angle between the observer and the source. The difference between the position of the source and the image then can be given by:

$$I - \eta = D_{OS} \tan \theta - D_{OS} \tan \beta = D \frac{\sin \alpha}{\cos \beta}, \quad (1)$$

where  $D_{OS}$  is the distance from the observer to the source, and  $D$  is the radial distance between the source and the point of the ray's closest approach. In most astrophysical cases where the distance between the source, the observer, and the lens are very large in comparison to the size of the objects in question, this radial distance can be approximated by  $D_{LS}$  - the distance between the lens and the source. This allows simplification of Eq 1 to (Mollerach & Roulet 2002):

$$\theta D_{OS} = \beta D_{OS} - \hat{\alpha} D_{LS}. \quad (2)$$

Dividing through by  $D_{OS}$ , and folding  $\hat{\alpha} \frac{D_{LS}}{D_{OS}}$  into a  $\alpha$ , where  $\hat{\alpha}$  is referred to as the reduced deflection angle, yields the standard lens equation (Mollerach & Roulet 2002):

$$\theta = \beta - \alpha \quad (3)$$

## 2.2. Magnification and Amplification

As introduced above, lensing involves the deflection of rays; i.e. it is not a process of absorption or emission, so no change in intensity will occur. The distances between lens, observer, and the source are also essentially constant, which means that we can assume no change in the surface brightness of the source. What is changing, however, is the solid angle of the source images produced by the deflection - i.e. lensing is a magnification process. For light, the flux received from an object may be expressed as a product of the surface brightness and solid angle (at least in the limit where the solid angle,  $\Delta\omega$ , is small) which means that the ratio of the fluxes, for the lensed and unlensed case, reduces to the ratio of the lensed to unlensed solid angle, yielding a factor that describes the amount of magnification. This ratio,  $\mu$ , is known as the *magnification factor* (Schneider et al. 2013):

$$\mu = \frac{\Delta\omega}{(\Delta\omega)_0}. \quad (4)$$

In the gravitational wave case there is an equivalent change in wave amplitude produced by lensing, and an equivalent ratio between the unlensed and lensed cases which indicates the *amplification factor*

$$F(w, \boldsymbol{\eta}) = \frac{\phi_{obs}^L(w, \boldsymbol{\eta})}{\phi_{obs}(w, \boldsymbol{\eta})}. \quad (5)$$

Here  $w$  is a dimensionless frequency, and  $\boldsymbol{\eta}$ , as previously defined, is the position of the source. Because the parameters characterising a gravitational wave signal and - with the exception of the frequency - the parameters defining this amplification factor are uncorrelated, the relationship between the lensed and unlensed gravitational-wave strain takes the following simple form (Takahashi & Nakamura 2003):

$$h^L(f) = h(f) \times F(f). \quad (6)$$

## 2.3. Multiple Images

As was already mentioned, lensing can produce multiple images. Consider, for example, the simplest type of lensing object which can be considered to be a point mass. In this case, the reduced deflection angle from the lens equation is found to be (Mollerach & Roulet 2002):

$$\alpha = \frac{D_{LS}}{D_{OS} D_{OL}} \frac{4GM}{\theta c^2}. \quad (7)$$

To simplify the scenario further, consider also the case where the observer and the source both lie on the optical axis, i.e.  $\beta = 0$ . In this case, inserting Eq 7 into Eq 3 indicates that the image will form a ring, known as the Einstein Ring - the angular radius of which will be given by the Einstein Angle  $\theta_E$ . For the scenario that has been outlined here,  $\theta_E$  is given by (Mollerach & Roulet 2002)

$$\theta_E = \sqrt{\frac{D_{LS}}{D_{OS} D_{OL}} \frac{4GM}{c^2}}. \quad (8)$$

In the more general case in which  $\beta$  is non-zero, however, this equation yields a pair of images at two different angular positions given by (Mollerach & Roulet 2002):

$$\theta_{\pm} = \frac{\beta}{2} \pm \theta_E \sqrt{1 + \frac{\beta^2}{4\theta_E^2}}. \quad (9)$$

Similar considerations apply in the case of lenses that are extended mass distributions: in general the lens equation admits multiple solutions, corresponding to multiple image positions.

## 3. LENSING PROFILES

In the simple scenario considered previously, the lensing object was considered to be a point mass. However, in general, real world astrophysical objects are extended objects that are not uniform in density - information about which is encoded by a density profile  $\rho(\boldsymbol{x})$ . Thus, different density profiles result in different lensing signatures (Takahashi & Nakamura 2003), meaning that the lensing signature can in principle provide information on the density profile and determine whether a given model profile is consistent with the observed data. Such

analyses can ultimately, therefore, place important constraints on the nature of the lensing object.

For astrophysical sources, the distances between the lensing object, the source, and the observer are generally much larger than the thickness of the lensing object. This allows the so called thin-lens approximation to be applied: instead of requiring a fully three-dimensional density profile,  $\rho(\mathbf{x})$ , the surface mass density  $\Sigma(\xi)$  can be considered: this is the projection of the three-dimensional density onto a two-dimensional plane, perpendicular to the line-of-sight to the source and at the distance of the centre of mass of the lensing object, i.e.

$$\Sigma(\xi) = \int \rho(\xi, z) dz. \quad (10)$$

Should the extended mass distribution be spherically symmetric, this allows for some further simplification because the surface mass density depends only upon the modulus of the impact parameter,  $\xi = |\xi|$ . The deflection angle for the mass profile is then given by (Mollerach & Roulet 2002):

$$\hat{\alpha} = \frac{4GM(\xi)}{c^2\xi}, \quad (11)$$

where  $M(\xi)$  describes the amount of mass that is enclosed inside a circle of radius  $\xi$  on the projected plane. This is referred to as the reduced mass and is given by (Mollerach & Roulet 2002):

$$M(\xi) \equiv 2\pi \int_0^\xi \xi' \Sigma(\xi') d\xi'. \quad (12)$$

With the deflection angle given by Eq 11, this means that the lens equation is modified in this scenario to:

$$\beta = \theta - \frac{M(\theta)}{\pi D_{OL}^2 \theta \Sigma_{cr}}, \quad (13)$$

where  $\Sigma_{cr}$  is called the critical surface mass density and is given by (Schneider et al. 2013):

$$\Sigma_{cr} = \frac{c^2 D_{OS}}{4\pi G D_{OL} D_{OS}}. \quad (14)$$

There are a number of mass density profiles that are frequently used to describe extended distributions of matter. Two commonly used examples are the Singular Isothermal Sphere (SIS) (Robertson et al. 2020) and the Navarro, Frenk, and White (NFW) profiles (Navarro et al. 1997). These will be described in detail in the following section as they were chosen to be explicitly developed and included within GRAVELAMPS. However, there are a multitude of other density profiles considered in the literature, some of which will be commented on briefly at the end of this section.

### 3.1. Singular Isothermal Sphere

The Singular Isothermal Sphere, or SIS, profile is the simplest and most widely used profile that has been designed to model the behaviour most commonly observed for galaxies – i.e. a flat rotation curve. This behaviour arises as the result of modelling the galaxy as a large, extended object containing luminous matter embedded within a dark matter halo. Whilst the key strength of the SIS profile is its ability to replicate this flat rotation curve (Gavazzi et al. 2007), it does suffer from a weakness in the form of a central singularity which is non-physical (Burkert 1995) (Shi et al. 2021). The full SIS density profile is given by (Robertson et al. 2020):

$$\rho_{SIS}(r) = \frac{\sigma^2}{2\pi G r^2}, \quad (15)$$

where  $\sigma$  is the one-dimensional velocity distribution of stars around the galaxy being modelled. This leads to a surface mass density of (Robertson et al. 2020):

$$\Sigma_{SIS}(\xi) = \frac{\sigma^2}{2G\xi}, \quad (16)$$

which corresponds to a reduced mass that can be calculated analytically as (Robertson et al. 2020):

$$M_{SIS}(\xi) = \frac{\pi\sigma^2}{G}\xi. \quad (17)$$

### 3.2. Navarro, Frenk, and White Profile

In the standard Concordance Model of Cosmology (Aghanim et al. 2020) (Carroll 2001) the dark matter is assumed to be cold and collisionless. Consistent with these properties, the Navarro, Frenk, and White, or NFW, profile is widely used to model the density profile of cold dark matter (CDM) halos, as described by a singular ‘universal’ scaling function. Whilst allowing for more complexity than the Singular Isothermal Sphere profile, the NFW profile suffers from the same central singularity, or cusp. The density is given by (Navarro et al. 1997):

$$\rho_{NFW}(r) = \frac{r_s}{\frac{r}{r_s} \left(1 + \frac{r}{r_s}\right)^2}, \quad (18)$$

where  $\rho_s$  is the central density and  $r_s$  is the characteristic scale of the profile. This density profile leads to a surface mass density given by (Bartelmann 1996):

$$\Sigma_{NFW}(\xi) = \begin{cases} \frac{2r_s\rho_s}{x^2-1} \left[1 - \frac{2}{\sqrt{1-x^2}} \operatorname{arctanh} \sqrt{\frac{1-x}{1+x}}\right] & \text{if } x < 1 \\ \frac{2r_s\rho_s}{3} & \text{if } x = 1 \\ \frac{2r_s\rho_s}{x^2-1} \left[1 - \frac{2}{\sqrt{1-x^2}} \operatorname{arctan} \sqrt{\frac{x^2-1}{1+x}}\right] & \text{if } x > 1 \end{cases}, \quad (19)$$

where in the assumed case of spherical symmetry,  $x = \xi/r_s$ . This then leads to a reduced mass of (Bartelmann 1996):

$$M_{NFW}(\xi) = 4\pi r_s \rho_s g(x), \quad (20)$$

where the function  $g(x)$  is given by:

$$g(x) = \begin{cases} \left[ \frac{2}{\sqrt{1-x^2}} \operatorname{arctanh} \sqrt{\frac{1-x}{1+x}} + \ln\left(\frac{x}{2}\right) \right] & \text{if } x < 1 \\ \left[ 1 + \ln\left(\frac{1}{2}\right) \right] & \text{if } x = 1 \\ \left[ \frac{2}{\sqrt{x^2-1}} \arctan \sqrt{\frac{x-1}{1+x}} + \ln\left(\frac{x}{2}\right) \right] & \text{if } x > 1 \end{cases} \quad (21)$$

### 3.3. Other Lensing Profiles

As was noted, both the Singular Isothermal Sphere and the Navarro, Frenk, and White profiles have the merits of a simple, universal mathematical description. However, they both share a central singularity which is non-physical and appears to be at odds with the observed properties of galaxies (Shi et al. 2021). There are however, other profiles which have been considered in the literature which do not share this issue. For instance, the Burkert profile (Burkert 1995) is similar to the NFW profile in that it is a simple scaling relation, but with a finite density core. It is considered a useful description of galaxy properties due to its agreement with the NFW profile at large radii.

Due principally to the ‘cuspieness’ problem that besets the SIS and NFW profiles, together with a number of other issues that have been recognised with standard CDM (Weinberg et al. 2015) (Perivolaropoulos & Skara 2021), several other models of dark matter have been considered in the cosmology literature that extend beyond CDM. For example, by considering dark matter as a more general scalar field one can construct a soliton for the central core profile which avoids the cusp singularity; this soliton form can be combined with an NFW-style tail to give a complete dark matter profile (Schive et al. 2014) (Herrera-Martín et al. 2019).

## 4. AMPLIFICATION FACTOR CALCULATION

As has been noted in the previous section, the relationship between an unlensed and a lensed signal is straightforward: the strain is simply multiplied by an amplification factor, the parameters defining which – with the exception of the frequency – are unconnected to those of the source wave. This simplicity makes lensing a potentially useful probe of dark matter since comparing lensed and unlensed predicted waveforms can, in principle, constrain the value of this amplification factor and hence

the parameters of the lens model. In practice, however, this process can be more complicated because of model parameter degeneracies: i.e. different lens models may predict, for particular choices of source and lens model parameters, very similar lensed waveforms. Furthermore, it may also be the case that lensed waveforms, for particular lens and source parameters, closely resemble *unlensed* waveforms with different source parameters (Cao et al. 2014). A key goal for GRAVELAMPS is to provide the computational infrastructure to investigate quantitatively such cases.

Whilst the value of the amplification factor is dependent upon the lensing profile, it can be calculated from a general expression (Takahashi & Nakamura 2003):

$$F(w, y) = \frac{w}{2\pi i} \int d^2x \exp[iwT(x, y)], \quad (22)$$

where  $T(x, y)$  is the dimensionless time delay. The simplest form of this general expression is for the case of an axially-symmetric lensing object, where it is given by (Takahashi & Nakamura 2003):

$$F(w, y) = -iwe^{iwy^2/2} \int_0^\infty dx x J_0(wxy) m \times \exp\left[iw\left(\frac{1}{2}x^2 - \psi(x) + \phi_m(y)\right)\right], \quad (23)$$

where  $\psi(x)$  is the lensing potential,  $\phi_m(y)$  is the phase for the minimum time delay – this is chosen such that the minimum time delay is zero – and  $w$  is the dimensionless frequency defined by (Takahashi & Nakamura 2003):

$$w = \frac{D_{OS}}{D_{LS}D_{OL}} \xi_0^2 (1 + z_l) \omega, \quad (24)$$

and  $y$  is a dimensionless form of the source position,  $\boldsymbol{\eta}$  given by (Schneider et al. 2013):

$$y = \frac{D_L}{\xi_0 D_S} \boldsymbol{\eta}. \quad (25)$$

### 4.1. Geometric Optics Approximation

The geometric optics limit is that, in the case of very high dimensionless frequency (i.e.  $w \gg 1$ ), the stationary points of the dimensionless time delay are the only contributors to the amplification factor integral. This means that the image positions  $x_j$  are determined from the lens equation such that (Schneider et al. 2013):

$$\mathbf{y} = \mathbf{x} - \nabla_x \psi(x). \quad (26)$$



Expanding  $T(\mathbf{x}, \mathbf{y})$  around the  $j^{\text{th}}$  image position,  $x_j$  gives

$$\begin{aligned} (\mathbf{x}, \mathbf{y}) &= T(\mathbf{x}_j, \mathbf{y}) + \sum_a \partial_a T(\mathbf{x}_j, \mathbf{y}) \tilde{x}_a \\ &+ \frac{1}{2} \sum_{a,b} \partial_a \partial_b T(\mathbf{x}_j, \mathbf{y}) \tilde{x}_a \tilde{x}_b + \mathcal{O}(x^3), \end{aligned} \quad (27)$$

where  $\tilde{x} = \mathbf{x} - \mathbf{x}_j$  and the indices  $a, b$  run from 1 to 2. It follows immediately that the second term vanishes due to the fact that  $x_j$  is the stationary point of  $T(\mathbf{x}, \mathbf{y})$ . Inserting this into Equation 22, and using the Gaussian integral

$$\int_{-\infty}^{\infty} dx e^{iax^2} = \sqrt{\frac{\pi}{|a|}} e^{i\pi/4 \times \text{sign}(a)}, \quad (28)$$

finally yields the geometric optics approximation of the amplification factor (Nakamura & Deguchi 1999):

$$F_{geo}(w, y) = \sum_j |\mu_j|^{1/2} \exp[iwT_j - i\pi n_j], \quad (29)$$

where  $\mu_j$  denotes the magnification of the  $j^{\text{th}}$  image,  $T_j = T(\mathbf{x}_j, \mathbf{y})$ , and  $n_j = 0, 1/2, 1$  when  $\mathbf{x}_j$  is a minimum, saddle point, or maximum of  $T(\mathbf{x}, \mathbf{y})$  respectively.

#### 4.2. Point Mass Lens

As previously noted, the point mass is the simplest possible lens case. It is applicable in cases of compact objects such as stars or black holes, but it can also be used for extended objects, by means of the Birkhoff Theorem, in the case where the lens size is much smaller than the Einstein radius. It is one of the only cases in which the full wave optics calculation of the amplification factor, i.e. Equation 23, can be calculated analytically. Here the normalisation constant  $\xi_0$  in Equation 24 corresponds to the Einstein radius, given by:

$$\xi_0 = \left( \frac{4M_L D_{OL} D_{LS}}{D_{OS}} \right)^{1/2}. \quad (30)$$

This leads to the dimensionless frequency being given by  $w = 4M_{Lz}\omega$ , where  $M_{Lz}$  is the redshifted lens mass. This ultimately leads to the amplification factor in the full wave optics case being given by (Takahashi & Nakamura 2003):

$$\begin{aligned} F(w, y) &= \exp \left[ \frac{\pi w}{4} + i \frac{w}{2} \left\{ \ln \left( \frac{w}{2} - 2\phi_m(y) \right) \right\} \right] \\ &\times \Gamma \left( 1 - \frac{i}{2} w \right) {}_1F_1 \left( \frac{i}{2} w; 1; \frac{i}{2} w y^2 \right), \end{aligned} \quad (31)$$

where  ${}_1F_1$  is the confluent hypergeometric function of the first kind, and  $\phi_m(y)$  is given by  $(x_m - y)^2/2 - \ln x_m$  where  $x_m = (y + \sqrt{y^2 + 4})/2$ . In the geometric optics approximation case, the amplification factor is given by (Takahashi & Nakamura 2003)

$$F_{geo}(w, y) = |\mu_+|^{1/2} - i|\mu_-|^{1/2} e^{iw\Delta T}, \quad (32)$$

where the magnifications are given by  $\mu_{\pm} = 1/2 \pm (y^2 + 2)/(2y\sqrt{y^2 + 4})$  and the time delay between the two images is given by  $\Delta T = y\sqrt{y^2 + 4}/2 + \ln((\sqrt{y^2 + 4} + y)/(\sqrt{y^2 + 4} - y))$ .

#### 4.3. Singular Isothermal Sphere

The Singular Isothermal Sphere is more complicated than the point mass, but is still the simplest profile used to model extended objects. The SIS profile is defined by its velocity dispersion,  $v$ , and the normalisation constant chosen for the profile, similar to the point mass case, is the Einstein Radius, which for the SIS is given by (Takahashi & Nakamura 2003):

$$\xi_0 = 4\pi v^2 \frac{D_L D_{LS}}{D_S}. \quad (33)$$

The redshifted lens mass in the SIS profile is given by (Takahashi & Nakamura 2003):

$$M_{Lz} = 4\pi v^4 \left( 1 + z_l \right) \frac{D_L D_{LS}}{D_S}, \quad (34)$$

resulting in a consistent definition of the dimensionless frequency,  $w$ , as with the point mass. The amplification factor can be made simpler than directly calculating the integral in Equation 23 by first inserting that  $\psi(\mathbf{x}) = |\mathbf{x}|$  and then expanding the second term in the exponential into an infinite sum, yielding :

$$\begin{aligned} F(w, y) &= -iwe^{\frac{i}{2}wy^2 + iw\phi_m(y)} \\ &\times \sum_{n=0}^{\infty} \frac{(-iw)^n}{n!} \int_0^{\infty} x^{1+n} J_0(wxy) e^{\frac{i}{2}iwx}. \end{aligned} \quad (35)$$

This equation can then be solved, and using the identity that  $e^z {}_1F_1(a, b; -z) = {}_1F_1(a, b; z)$  (Abramowitz & Stegun 1965), this ultimately yields:

$$\begin{aligned} F(w, y) &= e^{\frac{i}{2}w(y^2 + 2\phi_m(y))} \sum_{n=0}^{\infty} \frac{\Gamma(1 + \frac{n}{2})}{n!} \\ &\times \left( 2we^{i\frac{3\pi}{2}} \right)^{n/2} {}_1F_1 \left( 1 + \frac{n}{2}, 1; -\frac{i}{2}wy^2 \right), \end{aligned} \quad (36)$$

where  $\phi_m(y) = y + 1/2$ . In the geometric optics case, the source position determines the number of images that

will be formed. If  $y < 1$  double images occur, where if  $y \geq 1$  only a single image is formed meaning that the amplification factor is split between these cases, being given by (Takahashi & Nakamura 2003):

$$F_{geo}(w, y) = \begin{cases} |\mu_+|^{1/2} - i|\mu_-|^{1/2}e^{iw\Delta T} & \text{for } y < 1 \\ |\mu_+|^{1/2} & \text{for } y \geq 1 \end{cases}, \quad (37)$$

where in this case, the magnifications are given by  $\mu_{\pm} = \pm 1 + 1/y$  and the time delays are given by  $\Delta T = 2y$ .

#### 4.4. Navarro, Frenk, White

Of the profiles considered in this work, the Navarro, Frenk, White profile is the most complicated. In addition to the amplification factor having to be calculated numerically, the time delay constant  $\phi_m(y)$  must also be calculated numerically due to the lens equation no longer having an analytical solution. The lensing potential also takes a more complicated form given by (Takahashi 2004):

$$\psi(x) = \frac{\kappa_s}{2} \begin{cases} \left[ \left( \ln \frac{x}{2} \right)^2 - (\operatorname{arctanh} \sqrt{1-x^2})^2 \right] & \text{for } x \leq 1 \\ \left[ \left( \ln \frac{x}{2} \right)^2 + (\operatorname{arctan} \sqrt{x^2-1})^2 \right] & \text{for } x \geq 1 \end{cases}. \quad (38)$$

Here,  $\kappa_s$  is the dimensionless surface density given by  $16\pi\rho_s(D_L D_{LS}/D_S)r_s$ . In the case of the NFW profile, the scale radius  $r_s$  is chosen instead of the Einstein Radius for the normalisation constant  $\xi_0$ . As previously mentioned the lens equation is not analytically solvable. This means that the image positions and therefore the time delays and magnifications must all be calculated numerically from the lens equation. Hence, the geometric optics amplification factor is calculated directly from Equation 29. In this case the number of images formed is dependent upon the value of  $y$  relative to a critical value – with three images being formed where  $|y| < y_{cr}$  and only one in the case where  $|y| > y_{cr}$ . In the case of the source position being at the critical value, the magnification becomes infinite.

## 5. GRAVELAMPS OVERVIEW

GRAVELAMPS is an analysis pipeline designed to study an arbitrary lensed gravitational-wave source and constrain properties of both the source and the mass density profile of the lens. The pipeline estimates the Bayesian evidence for a particular lens model, relative to that for other lens models or the unlensed hypothesis. In so doing, it also allows inference of both the source and lens parameters for the model(s) under consideration. The

application of GRAVELAMPS to some example scenarios, to illustrate its usefulness for identifying and characterising lensed gravitational-wave signals, will be presented in the following sections.

### 5.1. Languages and Toolkits Used

For the higher level parts – in terms of interacting with the user and performing the parameter estimation, GRAVELAMPS is coded in PYTHON. This allows for flexibility and ease of reading as well as access to a number of useful modules. In use in GRAVELAMPS are the extensively used NUMPY (Harris et al. 2020), SCIPY (Virtanen et al. 2020), and ASTROPY (The Astropy Collaboration et al. 2018) modules. Most importantly, the use of PYTHON gives access to the BILBY package (Ashton et al. 2019) thus ensuring the use of both reliable parameter estimation methods and native and easily extensible support for LAL waveforms. This creates a more cohesive experience for a user wishing to modify the program beyond the level of the options already available to them. The use of BILBY also allows the pipeline to be scaled straightforwardly for usage on clusterised machines, through BILBY\_PIPE (Romero-Shaw et al. 2020). In particular, there is little difference between a run designed to be implemented on a local machine and one designed for a clusterised machine, e.g. to be submitted through the scheduler HTCONDOR, as is used widely in the LSC clusters.

For the lensing data generation, as can be seen in the previous section, the amplification factor calculation is not a simple task as it requires the calculation of the integral of a highly oscillatory function. Due to the intensive nature of the calculations, these were coded in C++ to benefit from the additional speed of a compiled language – as well as granting access to the C arbitrary precision library ARB (Johansson 2017). In addition to being able to perform the necessary calculations with appropriate speed and accuracy, this approach had the benefit of allowing users to decide for themselves how much they wished to trade said speed and accuracy, as well as allowing the full wave optics to be calculated to as high a dimensionless frequency value as possible – well past the point at which the geometric optics approximation can successfully take over – without causing disruption to the amplification factor that is calculated.

In addition to those toolkits used directly in GRAVELAMPS, there are other pieces of software which are critical to the functioning of the toolkits themselves – with the BILBY package additionally depending upon such packages as MATPLOTLIB (Hunter 2007) and CORNER (Foreman-Mackey 2016) for plotting, and GWPY (Macleod et al. 2021) and LALSUITE (LIGO Scientific

(Collaboration 2018) for gravitational wave data analysis. Further, GRAVELAMPS allows the use of a great many samplers: chosen for the work presented here was DYNESTY (Speagle 2020).

### 5.2. Design Intentions

As with almost all software packages, there were certain philosophies which underpinned how the software was constructed, in addition to the obvious requirements of functionality and speed. In the case of GRAVELAMPS, the following were the most important considerations:

1. *Openness*: With such complicated integrals being necessary to perform the calculations to generate the amplification factor, it is tempting to consider platforms such as MATHEMATICA which are designed to tackle extremely complex mathematics easily and with speed. However, a problem with such platforms is their proprietary nature. GRAVELAMPS is designed to be open for use in as many applications as possible without any licensing conflicts; as such the toolkits used were chosen to reflect this, as well as the license chosen for GRAVELAMPS itself – with the source code for all of these being freely available.
2. *Simplicity*: In the spirit of the openness with which GRAVELAMPS was designed, it was also designed to be as understandable to the user as possible. In particular, the code was designed with ease of readability in mind, and so that interactions with the software by the user should be as simple as possible. As such, there is little difference between a run on a local machine and that on a cluster – requiring only manipulation of the configuration INI file.
3. *Extensibility*: Whilst at this time, only the three density profiles discussed in detail in this paper are fully coded, GRAVELAMPS as a platform is designed to be easily extensible – for example by including other density profiles or by considering multiple lenses.

### 5.3. Structure of an Analysis Run

Having been designed to be relatively simple, GRAVELAMPS does not require that the user in any way modify the backend, in order to carry out an analysis run; instead the user may select all necessary settings through means of a simple INI file – contained within which there are options governing:

- The output information

- Lens generation, including whether to directly generate or to read in previously computed files, as well as associated settings such as arithmetic precision
- HTCONDOR settings for clusterised runs
- BILBY\_PIPE settings for clusterised runs
- Common analysis options such as the waveform model adopted, trigger time chosen, etc
- Whether or not to perform an unlensed analysis, and if so, the associated settings to be used
- Event/Injection parameters
- Sampler settings

Hence the user is given as much control over the run as possible without the requirement of delving into the code and modifying it for each analysis – although the latter is, of course, possible too. With a completed INI, the next step for the user is to simply call the analysis function giving the INI as the sole argument. The two calls determine only whether the run is to be performed locally, or if not to create the necessary submit files for the HTCONDOR Scheduler. These calls are referred to as `gravelamps_local_inference` and `gravelamps_pipe_inference` respectively.

Should users be implementing a clusterised version of the code, they will receive a DAG file that will call each of the necessary submit files in order. If running locally, the steps will be carried out directly. From the point at which the analysis run begins, the procedure is as follows:

1. Over the specified ranges of the dimensionless frequency and source position, generate a grid of values of the amplification factor for the chosen lens model
2. Generate an interpolating function to evaluate the amplification factor for any given dimensionless frequency and source position within the specified ranges
3. Generate injection data/ Fetch event data – i.e. prepare the data that will be analysed
4. Run parameter estimation on the data using the chosen lensed waveform model

This procedure results in acquiring both estimates of the lens and source parameters for the given model, and also an estimate of the evidence for that model.



This can then be compared with the evidences for other models to give a quantitative indication of the preferred model. This latter step may include, if the user wishes, an estimate of the evidence for an unlensed model. In this unlensed case, however, GRAVELAMPS should not be considered as providing a true Bayes factor for the relative probability of the lensed and unlensed hypotheses since no explicit evaluation of any selection effects relevant to the lensed-to-unlensed posterior odds ratio is carried out, based on e.g. a numerical injection study that models the probability of ‘false positives’ – i.e. pairs of candidate gravitational-wave events with parameters that could be consistent with them being strongly-lensed multiple images of a single source (The LIGO Scientific Collaboration & The Virgo Collaboration 2021). In its current form, GRAVELAMPS conducts lens and source model parameter estimation on only a single such image. In the future we plan to explore its extension to the framework appropriate for analysis of multiple images, but in the remainder of this work we consider only the single image case.

#### 5.4. Package Structure

Following the standard PYTHON package layout of submodules with specific purposes in mind, GRAVELAMPS is split into `gravelamps.inference` and `gravelamps.lensing` covering the performance of the inference runs and the lensed waveform generation respectively.

##### 5.4.1. *gravelamps.inference*

Contained within `gravelamps.inference` are the individual scripts that form the programs by which the user interacts with GRAVELAMPS, i.e. `gravelamps_local_inference` and `gravelamps_pipe_inference`. In addition to the programs themselves, contained with `gravelamps.inference` are all of the functions which are concerned with handling the user’s configurations as well as the generation of the HTCONDOR submit files for the clusterised code. These are contained within the `helpers` and `file_generators` parts of the submodule.

##### 5.4.2. *gravelamps.lensing*

Contained within the PYTHON parts of `gravelamps.lensing` are the utility functions that pertain to the construction of the lensed waveform directly, such as generating the dimensionless frequency and source position data over which the interpolation will take place, as well as taking the base unlensed LAL waveforms and turning them into the corresponding lensed versions. In addition, `gravelamps.lensing`

contains those functions which perform physical calculations such as unit conversion, etc, whereas those calculations in `gravelamps.inference` are more statistical in nature.

In addition to the full analysis programs contained within `gravelamps.inference`, there is also a program contained within `gravelamps.lensing`. This program is `gravelamps.generate_lens` which comes in a `local` and `pipe` variant – allowing the generation of only the lensed data without analysis, which could for instance be used to generate one large data set from which multiple runs can be analysed.

In addition to the actual PYTHON submodule, `gravelamps.lensing` contains the source codes from which the programs that generate the amplification factor data are constructed. These programs are compiled upon the installation of GRAVELAMPS. Each of these programs functions in a similar manner: taking as inputs dimensionless frequency and source position information contained within unique file – together with some user defined settings, such as the point at which to switch to geometric optics or the arithmetic precision of the wave optics calculations. Each program returns two unique files containing the amplification factor’s real and imaginary values, which can then be fed into the PYTHON in order to generate a complex interpolator – allowing for speedy retrieval of the values.

The ability to implement both the wave optics and geometric optics calculations is particularly useful, in view of the complexity of the calculations required for the full wave optics analysis. Whilst these can be run for higher values of the dimensionless frequency, the calculation requires ever increasing precision and greater numerical limits on the integrations and summations; this leads to an increasing slow down due to the necessity of performing more calculations to reach these higher thresholds. However, GRAVELAMPS has been written in a sufficiently flexible state to leave this choice to the user rather than making it for them.

## 6. EXAMPLE USES OF GRAVELAMPS

One of the major focuses of GRAVELAMPS is to be as versatile in terms of how it can be used to study lensing of gravitational wave signals. As such, the lensing data can be generated by themselves, i.e. simulated data can be analysed, as well as real data. The following will cover examples of each of these use cases to demonstrate how an analysis might be made.

### 6.1. Generation of Amplification Factor Data

As was discussed in the previous sections, the generation of a lensed waveform from an unlensed one is simply

a matter of multiplying the strains of the unlensed waveform by the amplification factor function corresponding to the lensing model of interest. Calculation of that amplification factor can be done in two ways: by considering the full wave optics approach or by implementing the geometric optics approximation. Both of these approaches have benefits and drawbacks.

Figures 1 - 6 show the results of using GRAVELAMPS lens generation codes for both the wave and geometric optics cases, up to a dimensionless frequency of  $w = 100$ , for each of the Point Lens, SIS, and NFW models to illustrate the differences and applicability of both calculation styles.

In the case of full wave optics, the calculations are obviously more complete. However, they are significantly more computationally intensive, requiring the use of arbitrary precision calculations as well as the use of numerical integration in the more complicated cases. Even the SIS - the simplest of the extended object models requires the approximation of an infinite sum to a finite degree. This makes the generation of the wave optics amplification factor slower - increasingly so at higher dimensionless frequency where in order to retain numerical stability of the result, greater limits need to be placed on the summations and integrations as well as increasing precision.

In the case of the geometric optics, the calculations are much simpler. However, strictly they are only applicable at higher dimensionless frequency as at lower dimensionless frequency values they do not replicate the behaviours of the full wave optics function - noting that in Figures 4 and 6, the damped oscillatory nature of the higher source position value curves are replaced with a single value that approximates the average of the oscillation. The simplicity of the calculation in this case does, however, pay off in significantly greater speed, and so geometric optics may be warranted in the higher dimensionless frequency regimes.

GRAVELAMPS was designed to be a versatile system however, so the user is given as much control over these calculations as possible. The user from the INI file used to generate the amplification factor data is able to specify:

- The minimum and maximum dimensionless frequency and source position
- How many dimensionless frequency and source position points to be generated for the interpolator
- The precision used in the arbitrary precision calculations

- The upper limit of the summation and integration used in the SIS and NFW models respectively
- The dimensionless frequency value at which to switch to the geometric optics approximation

These choices are given to the user to allow them to decide for themselves how much speed/accuracy trading that they wish to adopt. This also allows for a hybrid approach, in particular preventing the user from being forced to use e.g. geometric optics in all cases; if the user has the computational resources and time available they are able to continue using the wave optics approach to as high a dimensionless frequency as they wish. It should be noted, however, that the higher dimensionless frequency wave optics calculations become ever more computationally expensive in order to retain numerical stability. As a result of this, the user is recommended only to use the wave optics approach above  $w = 100 - 1000$  (prior to which point the geometric optics approximation is clearly valid) - at least in the case where they are planning to use a single lens generation for multiple parameter estimation runs where the justification of such computational expense may be split between the runs.

The flexibility of GRAVELAMPS extends to other features. The user is able to specify any terminal-callable process in the INI and also what arguments are needed, allowing the user the ability to generate new models easily, even without adding to GRAVELAMPS itself directly (although users are encouraged to incorporate any such new models into the codebase should they wish to do so). If the user chooses to use non-implemented models, they are able to use the `gravelamps_generate_lens` programs to then generate the amplification factor data. Placing the file location of the resultant files into the INI's optional input then allows these data to be accessed in inference runs.

## 6.2. Analysis of a Simulated Lensed GW150914-like Event

In this section we use GRAVELAMPS to simulate a lensed waveform, with source properties modelled on those of GW150914, as an extension of the waveform generation capabilities of BILBY - themselves wrappers for LAL - to give a wide variety of base, unlensed waveforms to which the generated amplification factor data can be applied. Selected here as an illustrative example is the IMRPHENOMXP waveform model (Pratten et al. 2021).

To make GRAVELAMPS more feature complete, it is also capable of simulating an event as one waveform, and then analysing it as another - allowing investigation

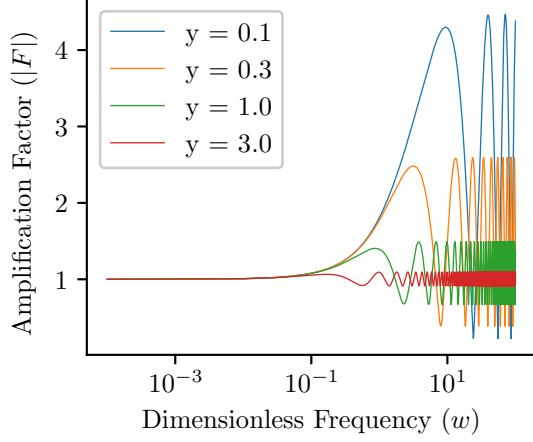


**Figure 1.** Absolute value of the amplification factor as calculated by GRAVELAMPS’ in-built generator for a point mass lens, using full wave optics at varying source positions.

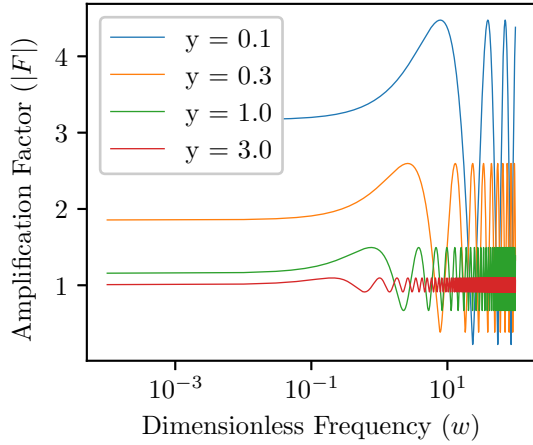


**Figure 2.** Absolute value of the amplification factor as calculated by GRAVELAMPS’ in-built generator for a point mass lens using geometric optics at varying source positions.

of the case where the wrong lensing profile is mistakenly applied. Moreover, as already highlighted, GRAVELAMPS is capable of generating predicted lensed waveforms under both geometric optics and wave optics scenarios.

The first analysis presented here simulates a GW150914-like event which is microlensed by a  $50M_{\odot}$  mass point lens, and is correctly analysed as a point-lensed event. The second and third analyses consider the GW150914-like event lensed by a  $4.4 \times 10^7 M_{\odot}$  Singular Isothermal Sphere, replicating a galaxy-scale ‘macrolensing’-type strong lensing event. This case was then modelled firstly as an SIS lens, and then as a NFW lens with scaling constant  $k_s = 2$  respectively. In both

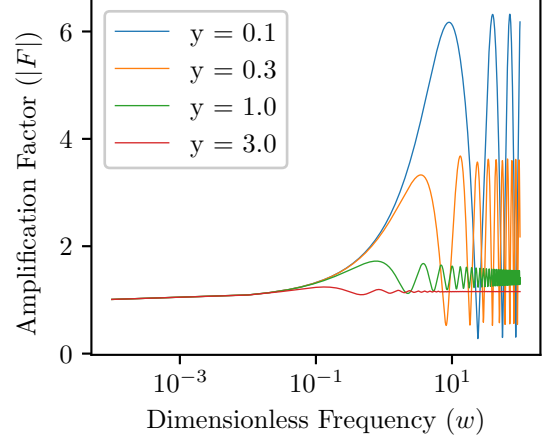


**Figure 3.** Absolute value of the amplification factor as calculated by GRAVELAMPS’ in-built generator for a Singular Isothermal Sphere style lens using full wave optics at varying source positions. Note the damped oscillations at higher source positions.

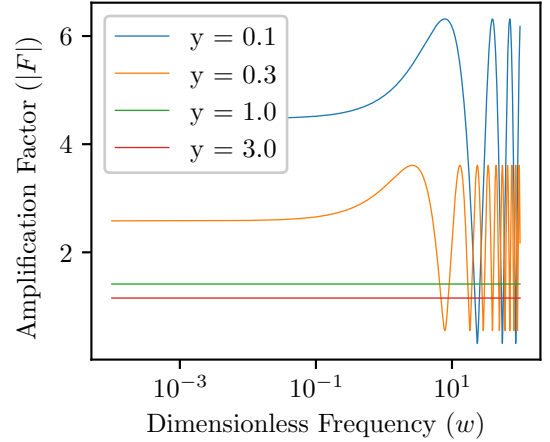


**Figure 4.** Absolute value of the amplification factor as generated by GRAVELAMPS’ in-built generator for a Singular Isothermal Sphere lens using geometric optics at varying source positions. Note here that instead of the damped oscillations, at higher source positions, the static oscillation is replaced with only a single (averaged) value.

cases, the lens has been placed at  $y = 1.0$  and placed half way between the source and the observer.

The true source properties used in each of these illustrative cases are summarised in Table 1 below.

Figure 7 shows the resulting parameter estimates inferred from the GRAVELAMPS simulation. As can be seen, each of the parameters has been recovered well; most are tightly constrained to ranges consistent with their true values. The least well-constrained parameter is the fractional lens luminosity distance to source lumi-

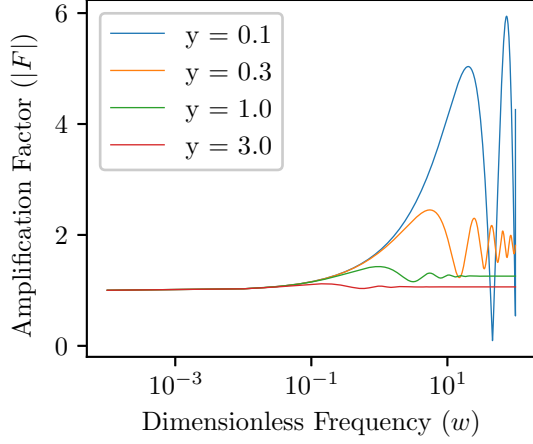


**Figure 5.** Absolute value of the amplification factor as calculated by GRAVELAMPS’ in-built generator for a Navarro, Frenk, White profile lens using full wave optics at varying source position. Note again the damped oscillations, which appear at lower source position values than in the SIS case

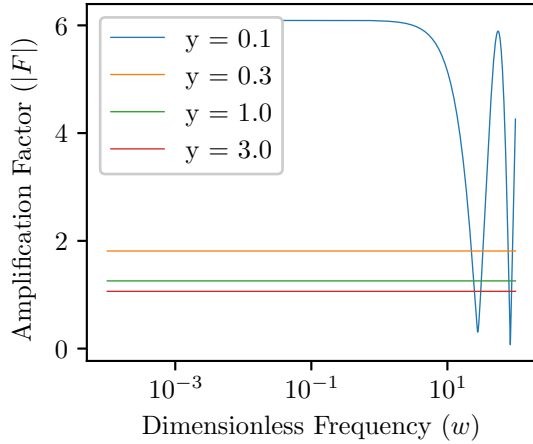


**Figure 6.** Absolute value of the amplification factor as calculated by GRAVELAMPS’ in-built generator for a Navarro, Frenk, White profile lens using geometric optics at varying source position. Note again that the damped oscillations have been replaced with a single value

nosity distance – although even in this case the posterior is informative and does peak at the correct value. Figure 8 shows the resulting parameter estimates from the GRAVELAMPS SIS macrolensing simulation. As can be seen, the parameters are still recovered – though they have wider posteriors as compared to the microlensing case, in particular in the lens mass. This is an expected result, as the inference of the lens mass is dependent upon the change of the amplification factor as a function of the dimensionless frequency (in which the lens mass is a contributing quantity); in the geometric op-

Parameter	Value
$m_1$	$36M_\odot$
$m_2$	$29M_\odot$
$a_1$	0.4
$a_2$	0.3
$\theta_1$	0.5 radians
$\theta_2$	1.0 radians
$\phi_{12}$	1.7 radians
$\phi_{Jl}$	0.3 radians
RA	1.375 radians
DEC	1.12108 radians
$d_L$	410 MPc
$\psi$	2.659
$t_c$	1126259642.413 GPS seconds

**Table 1.** Source parameters of the simulated GW150914-like gravitational wave event

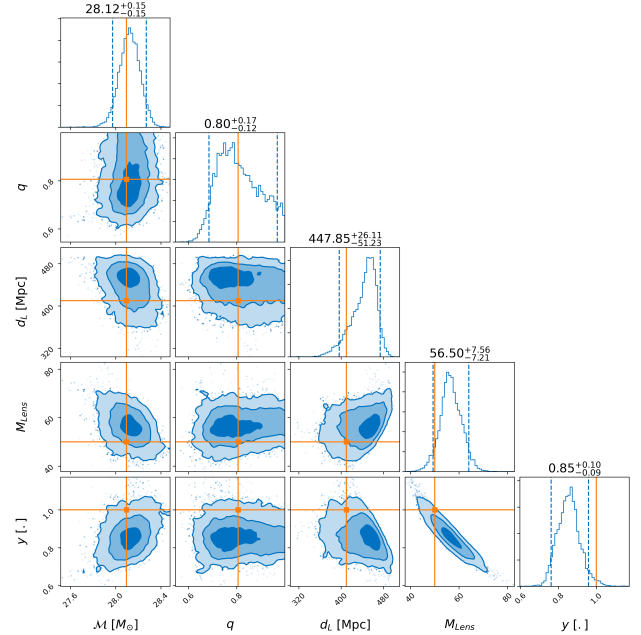


**Figure 7.** Results of lens and source model parameter estimation, performed by BILBY nested sampling using DYNESTY, for a GW150914-like gravitational-wave event microlensed by a  $50M_\odot$  mass point lens. As can be seen, GRAVELAMPS is able to successfully recover the model parameters, with most being well constrained. The least well-constrained parameter is the lens luminosity distance expressed as a fraction of the source luminosity distance; however the posterior is still informative.

tics case this amplification factor becomes a single value over all dimensionless frequency, so the lensed signal becomes insensitive to the lens mass.

Figure 9 shows the resulting parameter estimates from the third case, where the GW150914-like signal is lensed

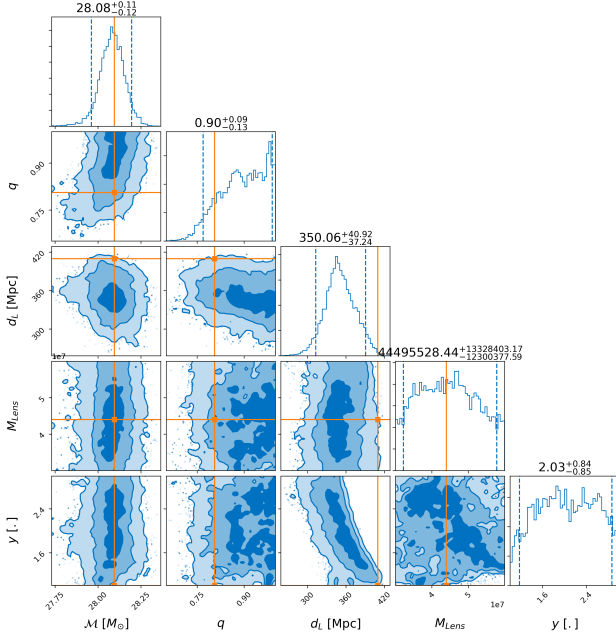


**Figure 8.** Results of lens and source model parameter estimation, performed by BILBY nested sampling using DYNESTY, for a GW150914-like gravitational-wave event lensed by a  $4.4 \times 10^7 M_\odot$  mass SIS lens – i.e. of typical scale for a galaxy macrolensing event. As can be seen, the parameters are reasonably well recovered, although it is clear that the precision of the parameter estimates is worse than the microlensing case

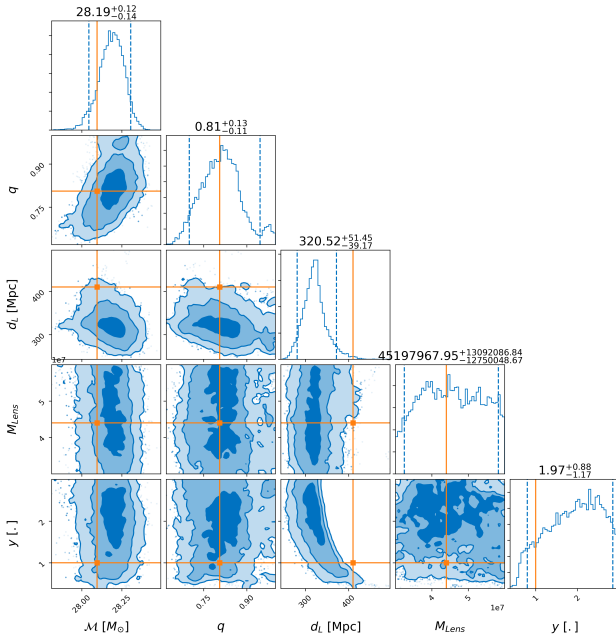


**Figure 9.** Results of lens and source model parameter estimation, performed by BILBY nested sampling using DYNESTY, for a GW150914-like gravitational-wave event lensed by a  $4.4 \times 10^7 M_\odot$  mass SIS lens, but analysed as an NFW lens.

by an SIS lens but is analysed as though it were lensed by an NFW profile. Most noticeable in this case is that the estimate for the luminosity distance is significantly less precise.

The second main goal for GRAVELAMPS is to be able to assess objectively the evidence for different lens models. In our macrolensing example, the log Bayes Factor of signal vs noise for analysing the event as SIS (the correct model) was  $14127.433 \pm 0.323$  and for the analysis of the event as NFW (the incorrect model) the log Bayes Factor was  $14110.538 \pm 0.327$ , yielding the log Bayes Factor comparing the SIS and NFW cases as 16.895 and thus strongly favours the SIS model. Hence the correct model was indeed strongly preferred in this case, despite the poorer performance of the parameter estimation on that model than was the case for our microlensing example.

### 6.3. Analysis of Real Event GW170809

To further illustrate of the usefulness of GRAVELAMPS and its suitability for analysis of real gravitational-wave event candidates, the real gravitational-wave event GW170809 was next analysed under the hypothesis that this event was lensed by an SIS and NFW profile respectively – with prior ranges for each model reflecting a galaxy mass-scale lens. This event was chosen due to the fact that, of those events analysed from the second observing run – from which the data is available from the Gravitational Wave Open Science Center (GWOSC) (Rich Abbott et al. 2021) – GW170809 was identified as one of the strongest (albeit ultimately rejected) lensing candidates (Hannuksela et al. 2019). Consequently, there has also been some additional interest shown in this event as a potential lensed candidate (Broadhurst et al. 2019).

Figures 10 – 12 show the results of the GRAVELAMPS runs for GW170809, analysing the event as unlensed, and strongly lensed by an SIS and NFW lens respectively with the posteriors for the unlensed case given in Figure 10 being compatible with those from the GWOSC data, as would be expected. In this case, the log Bayes Factors – comparing the hypothesis of modelled signal + noise, versus that of pure noise – for the unlensed, SIS, and NFW cases are  $56.219 \pm 0.250$ ,  $56.775 \pm 0.258$ , and  $56.461 \pm 0.26$  respectively. We see, therefore, that the signal + noise hypothesis is strongly favoured – consistent, of course, with the fact that GW170809 was identified as a confident gravitational-wave detection on GWTC-1. However, the log Bayes factor for each of the lensed hypotheses is only very slighter larger than that for the unlensed hypothesis – consistent with the conclusions of (Hannuksela et al. 2019) which rejected GW170809 as



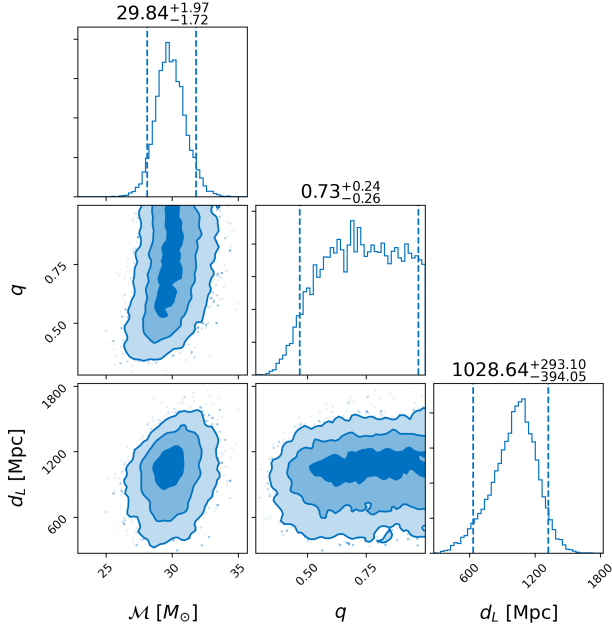


**Figure 10.** Results of lens and source model parameter estimation, performed by BILBY nested sampling using DYNESTY, for real event GW170809 using open data from GWOSC, and analysing the event as unlensed.

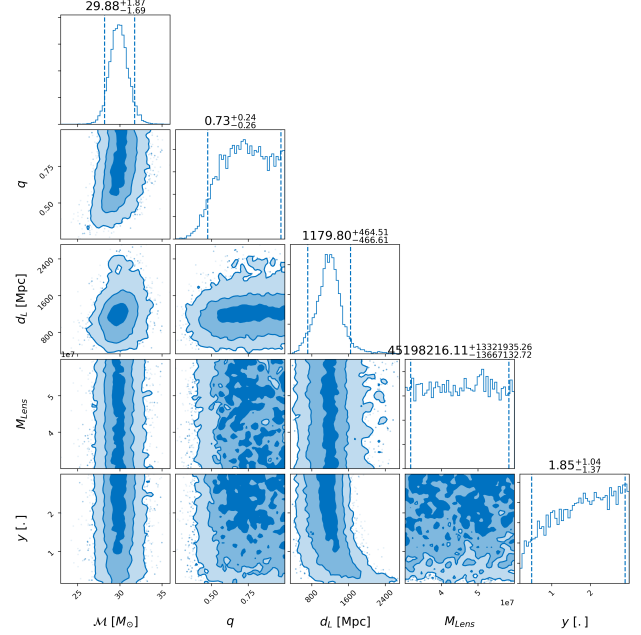


**Figure 12.** Results of lens and source model parameter estimation, performed by BILBY nested sampling using DYNESTY, for real event GW170809 using open data from GWOSC, and analysing the event as strongly lensed by an NFW profile.

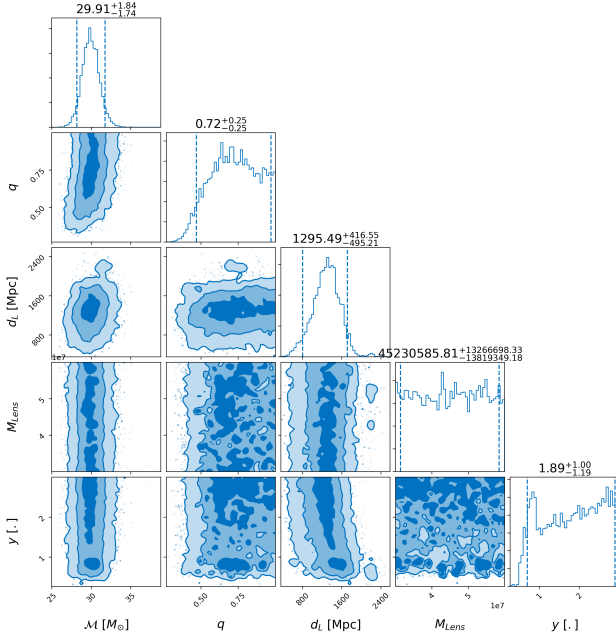


**Figure 11.** Results of lens and source model parameter estimation, performed by BILBY nested sampling using DYNESTY, for real event GW170809 using open data from GWOSC, and analysing the event as strongly lensed by an SIS profile.

a lensed event. Thus, while our GRAVELAMPS analysis does marginally favour the SIS lens model over the unlensed hypothesis, with a log Bayes factor of 0.556, and over the NFW model, with a log Bayes factor of 0.314, these results should be taken as merely illustrative of the capabilities of the software rather than any indication of a preference for a particular lens model in the case of GW170809. We emphasise again that GRAVELAMPS does not explicitly take into account the selection effects, multiple image analysis, and more detailed population prior choices that are explored in (The LIGO Scientific Collaboration & The Virgo Collaboration 2021), in order to better assess whether there is evidence supporting the lensing hypothesis for any given gravitational-wave candidate event. Nevertheless, we believe that the example of GW170809, and the previous simulated examples, illustrate the efficacy of GRAVELAMPS for comparing the evidence for different lens models *given* that a lensed gravitational-wave event has been detected.

## 7. CONCLUSION

With the increasing sensitivity of the existing ground-based detectors, and the additional detectors set to join the global network in the future, the detection of a lensed gravitational-wave event within a matter of a few years would appear to distinctly possible. Those searches performed thus far have focused on identifying candidate lensed events; however, once such a candidate

event has found, the immediately important question becomes what is the astrophysical nature of the lens itself? The package GRAVELAMPS presented here has been designed to help answer that question.

GRAVELAMPS has been designed to be an easy to use and versatile platform, with the flexibility to allow investigation of both microlensing scenarios, with lower mass point-mass lenses, and strong lensing by much higher-mass extended mass distributions such as the dark matter halos of galaxies and clusters. Equally accessible is the the so-called intermediate ‘mililensing’ case, and GRAVELAMPS is particularly adapted to this case by having the flexibility to calculate the lensing amplification factors in either geometric or wave optics, or in a hybrid combination of both, over the course of a single analysis run – with full control given to the user as to where each regime may apply. As an initial, illustrative, set of lensing models, GRAVELAMPS presently contains the point mass, Singular Isothermal Sphere, and Navarro, Frenk, White density profile; however it has been designed to easily be extended to include any lens model that the user wishes to investigate.

We have demonstrated the utility of GRAVELAMPS by presenting examples, in both of the wave and geometric optics cases, of its ability to infer parameters of both the lens and the source can be recovered – while noting the caveat that the performance does decrease in the geometric optics regime. However, even in this case, the model selection capabilities are still clear – with the estimated Bayes Factor strongly preferring the correct model. As noted, GRAVELAMPS is an easily extensible platform and the work presented here is seen as the just the first step in its development. For example, in future we plan to explore its extension to handle multiply lensed signals – for instance the case of a source

that simultaneously undergoes both microlensing and macrolensing.

## ACKNOWLEDGMENTS

The authors acknowledge computational resources provided by Cardiff University, and funding provided by STFC to support UK Involvement in the Operation of Advanced LIGO. MW acknowledges funding support provided by the Stirlingshire Educational Trust and the Scottish International Education Trust. MW is also grateful for the generous financial contribution of Mrs Catherine Goldie to this research. MH acknowledges additional support from the Science and Technology Facilities Council (Ref. ST/L000946/1). This research has made use of data, software and/or web tools obtained from the Gravitational Wave Open Science Center (<https://www.gw-openscience.org/>), a service of LIGO Laboratory, the LIGO Scientific Collaboration and the Virgo Collaboration. LIGO Laboratory and Advanced LIGO are funded by the United States National Science Foundation (NSF) as well as the Science and Technology Facilities Council (STFC) of the United Kingdom, the Max-Planck-Society (MPS), and the State of Niedersachsen/Germany for support of the construction of Advanced LIGO and construction and operation of the GEO600 detector. Additional support for Advanced LIGO was provided by the Australian Research Council. Virgo is funded, through the European Gravitational Observatory (EGO), by the French Centre National de Recherche Scientifique (CNRS), the Italian Istituto Nazionale di Fisica Nucleare (INFN) and the Dutch Nikhef, with contributions by institutions from Belgium, Germany, Greece, Hungary, Ireland, Japan, Monaco, Poland, Portugal, Spain. This material is based upon work supported by NSF’s LIGO Laboratory which is a major facility fully funded by the National Science Foundation.

## REFERENCES

- Aasi, J., Abbott, B. P., Abbott, R., et al. 2015, *Classical and Quantum Gravity*, 32, 074001, doi: [10.1088/0264-9381/32/7/074001](https://doi.org/10.1088/0264-9381/32/7/074001)
- Abbott, B., Abbott, R., Abbott, T., et al. 2019, *Physical Review X*, 9, doi: [10.1103/physrevx.9.031040](https://doi.org/10.1103/physrevx.9.031040)
- Abbott, B. P., Abbott, R., Abbott, T. D., et al. 2016, *Phys. Rev. Lett.*, 116, 061102, doi: [10.1103/PhysRevLett.116.061102](https://doi.org/10.1103/PhysRevLett.116.061102)
- . 2020, *Classical and Quantum Gravity*, 37, 055002, doi: [10.1088/1361-6382/ab685e](https://doi.org/10.1088/1361-6382/ab685e)
- Abbott, B. P., Abbott, R., Abbott, T. D., et al. 2021, *ApJ*, 909, 218, doi: [10.3847/1538-4357/abdcb7](https://doi.org/10.3847/1538-4357/abdcb7)
- Abbott, R., Abbott, T. D., Abraham, S., et al. 2021, *The Astrophysical Journal Letters*, 915, L5, doi: [10.3847/2041-8213/ac082e](https://doi.org/10.3847/2041-8213/ac082e)
- Abramowitz, M., & Stegun, I. A. 1965, *Handbook of mathematical functions with formulas, graphs, and mathematical tables*
- Acernese, F., Agathos, M., Agatsuma, K., et al. 2014, *Classical and Quantum Gravity*, 32, 024001, doi: [10.1088/0264-9381/32/2/024001](https://doi.org/10.1088/0264-9381/32/2/024001)
- Aghanim, N., Akrami, Y., Arroja, F., et al. 2020, *Astronomy & Astrophysics*, 641, A1, doi: [10.1051/0004-6361/201833880](https://doi.org/10.1051/0004-6361/201833880)

- Amorisco, N. C., Nightingale, J., He, Q., et al. 2021, Halo concentration strengthens dark matter constraints in galaxy-galaxy strong lensing analyses. <https://arxiv.org/abs/2109.00018>
- Ashton, G., Hübner, M., Lasky, P. D., et al. 2019, *ApJS*, 241, 27, doi: [10.3847/1538-4365/ab06fc](https://doi.org/10.3847/1538-4365/ab06fc)
- Bartelmann, M. 1996, *A&A*, 313, 697. <https://arxiv.org/abs/astro-ph/9602053>
- Belokurov, V., Evans, N. W., Moiseev, A., et al. 2007, *The Astrophysical Journal*, 671, L9–L12, doi: [10.1086/524948](https://doi.org/10.1086/524948)
- Broadhurst, T., Diego, J. M., & au2, G. F. S. I. 2019, Twin LIGO/Virgo Detections of a Viable Gravitationally-Lensed Black Hole Merger. <https://arxiv.org/abs/1901.03190>
- Burkert, A. 1995, *The Astrophysical Journal*, 447, doi: [10.1086/309560](https://doi.org/10.1086/309560)
- Cao, Z., Li, L.-F., & Wang, Y. 2014, *Phys. Rev. D*, 90, 062003, doi: [10.1103/PhysRevD.90.062003](https://doi.org/10.1103/PhysRevD.90.062003)
- Carroll, S. M. 2001, *Living Reviews in Relativity*, 4, doi: [10.12942/lrr-2001-1](https://doi.org/10.12942/lrr-2001-1)
- Chung, K.-W., & Li, T. G. F. 2021, Lensing of Gravitational Waves as a Novel Probe of Graviton Mass. <https://arxiv.org/abs/2106.09630>
- Cremonese, P., Ezquiaga, J., & Salzano, V. 2021, *Physical Review D*, 104, doi: [10.1103/physrevd.104.023503](https://doi.org/10.1103/physrevd.104.023503)
- Diego, J. M., Hannuksela, O. A., Kelly, P. L., et al. 2019, *A&A*, 627, A130, doi: [10.1051/0004-6361/201935490](https://doi.org/10.1051/0004-6361/201935490)
- Dyson, F. W., Eddington, A. S., & Davidson, C. 1923, *MmRAS*, 62, A1
- Einstein, A. 1916, *Sitzungsberichte der Königlich Preußischen Akademie der Wissenschaften* (Berlin), 688
- Ezquiaga, J. M., Holz, D. E., Hu, W., Lagos, M., & Wald, R. M. 2021, *Physical Review D*, 103, doi: [10.1103/physrevd.103.064047](https://doi.org/10.1103/physrevd.103.064047)
- Foreman-Mackey, D. 2016, *The Journal of Open Source Software*, 1, 24, doi: [10.21105/joss.00024](https://doi.org/10.21105/joss.00024)
- Gavazzi, R., Treu, T., Rhodes, J. D., et al. 2007, *ApJ*, 667, 176, doi: [10.1086/519237](https://doi.org/10.1086/519237)
- Hannuksela, O. A., Haris, K., Ng, K. K. Y., et al. 2019, *The Astrophysical Journal*, 874, L2, doi: [10.3847/2041-8213/ab0c0f](https://doi.org/10.3847/2041-8213/ab0c0f)
- Harris, C. R., Millman, K. J., van der Walt, S. J., et al. 2020, *Nature*, 585, 357, doi: [10.1038/s41586-020-2649-2](https://doi.org/10.1038/s41586-020-2649-2)
- Herrera-Martín, A., Hendry, M., Gonzalez-Morales, A. X., & Ureña-López, L. A. 2019, *The Astrophysical Journal*, 872, 11, doi: [10.3847/1538-4357/aafaf0](https://doi.org/10.3847/1538-4357/aafaf0)
- Hunter, J. D. 2007, *Computing in Science & Engineering*, 9, 90, doi: [10.1109/MCSE.2007.55](https://doi.org/10.1109/MCSE.2007.55)
- Janquart, J., Hannuksela, O. A., Haris, K., & Van Den Broeck, C. 2021, *Monthly Notices of the Royal Astronomical Society*, 506, 5430–5438, doi: [10.1093/mnras/stab1991](https://doi.org/10.1093/mnras/stab1991)
- Johansson, F. 2017, *IEEE Transactions on Computers*, 66, 1281, doi: [10.1109/TC.2017.2690633](https://doi.org/10.1109/TC.2017.2690633)
- LIGO Scientific Collaboration. 2018, *LIGO Algorithm Library - LALSuite*, free software (GPL), doi: [10.7935/GT1W-FZ16](https://doi.org/10.7935/GT1W-FZ16)
- Macleod, D. M., Areeda, J. S., Coughlin, S. B., Massinger, T. J., & Urban, A. L. 2021, *SoftwareX*, 13, 100657, doi: [10.1016/j.softx.2021.100657](https://doi.org/10.1016/j.softx.2021.100657)
- Mishra, A., Meena, A. K., More, A., Bose, S., & Bagla, J. S. 2021, *Gravitational Lensing of Gravitational Waves: Effect of Microlens Population in Lensing Galaxies*. <https://arxiv.org/abs/2102.03946>
- Mollerach, S., & Roulet, E. 2002, *Gravitational Lensing and Microlensing* (World Scientific). <https://books.google.co.uk/books?id=PAErrkpBYG0C>
- Mukherjee, S., Broadhurst, T., Diego, J. M., Silk, J., & Smoot, G. F. 2021, *Monthly Notices of the Royal Astronomical Society*, doi: [10.1093/mnras/stab1980](https://doi.org/10.1093/mnras/stab1980)
- Nakamura, T. T., & Deguchi, S. 1999, *Progress of Theoretical Physics Supplement*, 133, 137, doi: [10.1143/PTPS.133.137](https://doi.org/10.1143/PTPS.133.137)
- Navarro, J. F., Frenk, C. S., & White, S. D. M. 1997, *ApJ*, 490, 493, doi: [10.1086/304888](https://doi.org/10.1086/304888)
- Perivolaropoulos, L., & Skara, F. 2021, *Challenges for  $\Lambda$ CDM: An update*. <https://arxiv.org/abs/2105.05208>
- Pratten, G., García-Quirós, C., Colleoni, M., et al. 2021, *Physical Review D*, 103, doi: [10.1103/physrevd.103.104056](https://doi.org/10.1103/physrevd.103.104056)
- Rich Abbott, Thomas D. Abbott, Sheelu Abraham, et al. 2021, *SoftwareX*, 13, 100658, doi: <https://doi.org/10.1016/j.softx.2021.100658>
- Robertson, A., Smith, G. P., Massey, R., et al. 2020, *Monthly Notices of the Royal Astronomical Society*, 495, 3727, doi: [10.1093/mnras/staa1429](https://doi.org/10.1093/mnras/staa1429)
- Romero-Shaw, I. M., Talbot, C., Biscoveanu, S., et al. 2020, *Monthly Notices of the Royal Astronomical Society*, 499, 3295–3319, doi: [10.1093/mnras/staa2850](https://doi.org/10.1093/mnras/staa2850)
- Schive, H.-Y., Chiueh, T., & Broadhurst, T. 2014, *Nature Physics*, 10, 496–499, doi: [10.1038/nphys2996](https://doi.org/10.1038/nphys2996)
- Schneider, P. 1996, *Monthly Notices of the Royal Astronomical Society*, 283, 837, doi: [10.1093/mnras/283.3.837](https://doi.org/10.1093/mnras/283.3.837)
- Schneider, P., Ehlers, J., & Falco, E. 2013, *Gravitational Lenses*, *Astronomy and Astrophysics Library* (Springer Berlin Heidelberg). <https://books.google.co.uk/books?id=XJ3zCAAQBAJ>

- Seo, E., Hannuksela, O. A., & Li, T. G. F. 2021, Strong lensing: A magnifying glass to detect gravitational-wave microlensing. <https://arxiv.org/abs/2110.03308>
- Shi, Y., Zhang, Z.-Y., Wang, J., et al. 2021, *The Astrophysical Journal*, 909, 20, doi: [10.3847/1538-4357/abd777](https://doi.org/10.3847/1538-4357/abd777)
- Skilling, J. 2004, in *American Institute of Physics Conference Series*, Vol. 735, *Bayesian Inference and Maximum Entropy Methods in Science and Engineering: 24th International Workshop on Bayesian Inference and Maximum Entropy Methods in Science and Engineering*, ed. R. Fischer, R. Preuss, & U. V. Toussaint, 395–405, doi: [10.1063/1.1835238](https://doi.org/10.1063/1.1835238)
- Skilling, J. 2006, *Bayesian Analysis*, 1, 833 , doi: [10.1214/06-BA127](https://doi.org/10.1214/06-BA127)
- Speagle, J. S. 2020, *MNRAS*, 493, 3132, doi: [10.1093/mnras/staa278](https://doi.org/10.1093/mnras/staa278)
- Takahashi, R. 2004, PhD thesis, Department of Physics, Kyoto University, Japan. <http://cosmo.phys.hirosaki-u.ac.jp/takahasi/dt.pdf>
- Takahashi, R., & Nakamura, T. 2003, *The Astrophysical Journal*, 595, 1039–1051, doi: [10.1086/377430](https://doi.org/10.1086/377430)
- The Astropy Collaboration, Price-Whelan, A. M., Sipőcz, B. M., et al. 2018, *AJ*, 156, 123, doi: [10.3847/1538-3881/aabc4f](https://doi.org/10.3847/1538-3881/aabc4f)
- The LIGO Scientific Collaboration, & The Virgo Collaboration. 2021, Search for lensing signatures in the gravitational-wave observations from the first half of LIGO-Virgo’s third observing run. <https://arxiv.org/abs/2105.06384>
- The LIGO Scientific Collaboration, The Virgo Collaboration, Abbott, R., et al. 2021, GWTC-2.1: Deep Extended Catalog of Compact Binary Coalescences Observed by LIGO and Virgo During the First Half of the Third Observing Run. <https://arxiv.org/abs/2108.01045>
- Urrutia, J., & Vaskonen, V. 2021, Lensing of gravitational waves as a probe of compact dark matter. <https://arxiv.org/abs/2109.03213>
- Virtanen, P., Gommers, R., Oliphant, T. E., et al. 2020, *Nature Methods*, 17, 261, doi: [10.1038/s41592-019-0686-2](https://doi.org/10.1038/s41592-019-0686-2)
- Wang, J.-S., Herrera-Martín, A., & Hu, Y.-M. 2021, Lensing by primordial black holes: constraints from gravitational wave observations. <https://arxiv.org/abs/2108.12394>
- Weinberg, D. H., Bullock, J. S., Governato, F., Kuzio de Naray, R., & Peter, A. H. G. 2015, *Proceedings of the National Academy of Sciences*, 112, 12249, doi: [10.1073/pnas.1308716112](https://doi.org/10.1073/pnas.1308716112)
- Xu, F., Ezquiaga, J. M., & Holz, D. E. 2021, Please repeat: Strong lensing of gravitational waves as a probe of compact binary and galaxy populations. <https://arxiv.org/abs/2105.14390>